Examination of Effective Dielectric Constants of Nonspherical Mixed-Phase Hydrometeors

LIANG LIAO

Goddard Earth Sciences Technology and Research, and Morgan State University, Greenbelt, Maryland

ROBERT MENEGHINI

NASA Goddard Space Flight Center, Greenbelt, Maryland

(Manuscript received 25 November 2011, in final form 22 March 2012)

ABSTRACT

The validity of the effective dielectric constant $\varepsilon_{\mathrm{eff}}$ for nonspherical mixed-phase particles is tested by comparing the scattering parameters of ice–water mixtures for oblate and prolate spheroids obtained from the conjugate-gradient and fast Fourier transform (CGFFT) numerical scheme with those computed from the T matrix for a homogeneous particle with the derived $\varepsilon_{\mathrm{eff}}$ with the same size, shape, and orientation as that of the mixed-phase particle. The accuracy of the effective dielectric constant is evaluated by examining whether the scattering parameters of interest can reproduce those of the direct computations, that is, the CGFFT results. Computations have been run over a range of prolate and oblate spheroids of different axial ratios up to size parameters of 4. It is found that the effective dielectric constant, obtained from realizations of small particles, can be applied to a class of particle types if the fractional water content remains the same. Analysis of the results indicates that the effective dielectric constant approach is useful in computing radar and radiometer polarimetric scattering parameters of nonspherical mixed-phase particles.

1. Introduction

The bright band, a layer of enhanced radar echo associated with melting hydrometeors, is often observed in stratiform rain. The microphysical properties of melting hydrometeors and their scattering and propagation effects have long been studied not only because of their importance in accurately estimating parameters of the precipitation from spaceborne radar and radiometers but also as a result of their negative influence on earth–satellite communication systems caused by attenuation and depolarization of radio signals (Bringi et al. 1986; Fabry and Szymer 1999; Olson et al. 2001a,b; Meneghini and Liao 2000; Liao and Meneghini 2005; Sassen et al. 2005, 2007; Liao et al. 2009). To characterize the properties of the melting layer, a number of observations of the radar bright band have been made by both ground-based weather radars and multifrequency airborne radars. However, one of the impediments to the study of the radar signature of the melting layer is the determination of effective dielectric constants of melting hydrometeors. Although a number of mixing formulas are available to compute the effective dielectric constants, their results vary to a great extent when water is a component of the mixture, such as in the case of melting snow (Maxwell Garnett 1904; Bruggeman 1935). It is also physically unclear as to how to select among these various formulas. Furthermore, questions remain as to whether these mixing formulas can be applied to computations of radar polarimetric parameters from nonspherical melting particles.

Recently, several approaches using numerical methods have been developed to derive the effective dielectric constants of melting hydrometeors, that is mixtures consisting of air, ice, and water, based on more realistic melting models of particles, in which the composition of the melting hydrometeor is divided into a number of identical cells (Meneghini and Liao 1996, 2000; Liao and Meneghini 2005; Liao et al. 2009). Each of these cells is then assigned in a probabilistic way to be water, ice, or air according to the distribution of fractional water contents

Corresponding author address: Dr. Liang Liao, Goddard Earth Science Technology/MSU, Code 612, NASA Goddard Space Flight Center, Greenbelt, MD 20771.
E-mail: liang.liao-1@nasa.gov

DOI: 10.1175/JAMC-D-11-0244.1

© 2013 American Meteorological Society

for a particular particle. While the derived effective dielectric constants have been extensively tested at various wavelengths over a range of particle sizes, these numerical experiments have been restricted to the copolarized scattering parameters from spherical particles (Meneghini and Liao 1996, 2000; Liao and Meneghini 2005; Liao et al. 2009). As polarimetric radar has been increasingly used in the study of microphysical properties of hydrometeors, it will certainly provide additional information on melting processes. To account for polarimetric radar measurements from melting hydrometeors, it is necessary to move away from the restriction that the melting particles are spherical.

The primary goal of this study is to derive the effective dielectric constants of nonspherical mixed-phase particles. The computational model for the mixture is described by a collection of 128^3 cubic cells of identical size. Because of such a high-resolution model, the particles can be described accurately not only with regard to shape but with respect to structure as well. The Cartesian components of the mean internal electric field of the particle, which are used to infer the effective dielectric constants, are calculated at each cell by the use of the conjugate gradient-fast Fourier transform (CGFFT) numerical method. In this work, we first check the validity of derived effective dielectric constant from the nonspherical mixed-phase particle by comparing the scattering and polarimetric parameters of a mixture obtained from the CGFFT to those computed from analytical solutions for a homogeneous particle with the same geometry as that of the mixed-phase particle (such as size, shape, and orientation) with an effective dielectric constant derived from the internal field of the mixed-phase particle. The accuracy of the effective dielectric constant can be judged by whether the scattering parameters of interest can accurately reproduce those of the exact solution.

The purpose of the effective dielectric constant is to reduce the complexity of the scattering calculations in the sense that this quantity, once obtained, may be applicable to a range of particle sizes, shapes and orientations. Having computed the effective dielectric constant for a particle with a specific shape, size, and orientation, a check is performed to see if the result, obtained from one realization (with a fixed size, shape, and orientation), can be used to characterize a class of particle types (with arbitrary sizes, shapes, and orientations) if the fractional water contents of melting particles remain the same. Among the scattering and polarimetric parameters used for examination of the effective dielectric constant in this study are angular scattering intensity, radar backscattering, extinction and scattering coefficients, asymmetry factor, phase shift, and linear polarization ratio (LDR). The ultimate objective is to examine whether the effective dielectric constant approach provides a means to compute radar and radiometric polarimetric scattering parameters from the melting layer in a relatively simple and accurate way.

The paper is organized as follows. A definition of effective dielectric constant of a mixture and the associated equations are given in section 2, while the construction of nonspherical mixing particles is described in section 3. In section 4, tests of the derived effective dielectric constants from nonspherical mixtures are conducted and their utility in providing accurate scattering parameters is assessed. This is followed by the summary and remarks in section 5.

2. Effective dielectric constant

Let $\mathbf{E}(\mathbf{r}, \lambda)$ and $\mathbf{D}(\mathbf{r}, \lambda)$ be the local electric and dielectric displacement fields within a composite material at location $\mathbf{r}$ at free-space wavelength λ, satisfying

$$\mathbf{D}(\mathbf{r},\lambda) = \varepsilon(\mathbf{r},\lambda)\mathbf{E}(\mathbf{r},\lambda), \tag{1}$$

where ε is the dielectric constant. In view of the local constitutive law described by the above equation, the bulk effective dielectric constant $\varepsilon_{\mathrm{eff}}$ is defined as the ratio of the volume averages of $\mathbf{D}$ and $\mathbf{E}$ fields (Stroud and Pan 1978):

$$\varepsilon_{\mathrm{eff}} \iiint_V \mathbf{E}(\mathbf{r},\lambda)\, dv = \iiint_V \mathbf{D}(\mathbf{r},\lambda)\, dv. \tag{2}$$

If the particle, composed of two materials ε_1 and ε_2, is approximated by N small equal-volume elements, then the $\varepsilon_{\mathrm{eff}}$ can be written as

$$\varepsilon_{\mathrm{eff}} = \frac{\varepsilon_1 \sum_{j\in M_1} \mathbf{E}_j + \varepsilon_2 \sum_{j\in M_2} \mathbf{E}_j}{\sum_{j\in M_1} \mathbf{E}_j + \sum_{j\in M_2} \mathbf{E}_j}. \tag{3}$$

The notations $\sum_{\in M_1}$ and $\sum_{j\in M_2}$ denote summations over all the volume elements composing materials 1 and 2, respectively. The internal $\mathbf{E}$ fields appearing on the right-hand sides of (3) are in the same polarization as the incident wave. In this study, they are computed by the CGFFT numerical method (Catedra et al. 1995; Sarkar et al. 1986; Su 1989) in which the volume enclosing the total particle is divided into 128^3 identical cells. The CGFFT is one of the popular numerical schemes that are applied for solving the electromagnetic scattering problem from hydrometeors of arbitrary shapes and compositions. The CGFFT method solves the electric field integral equation derived from Maxwell's equations.

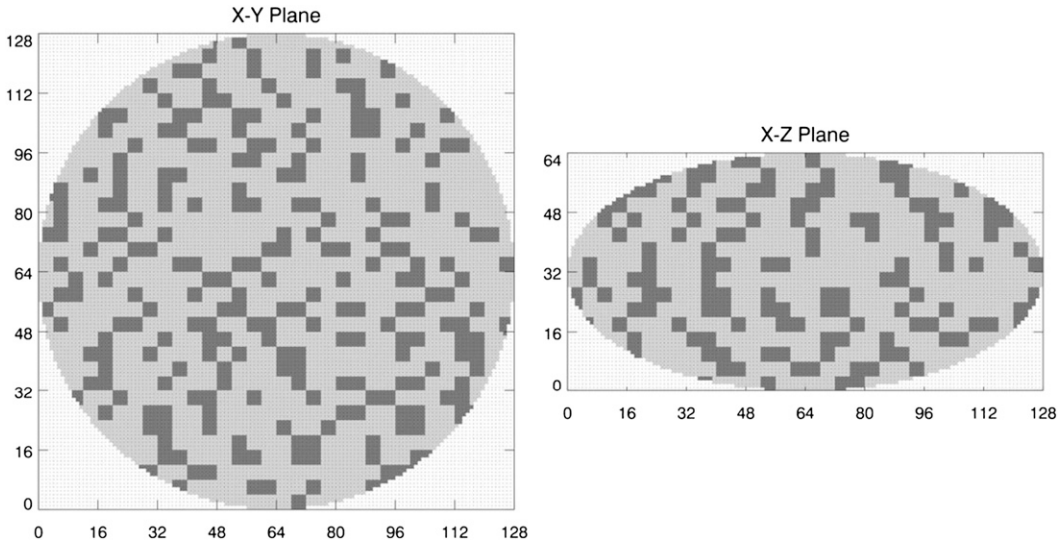

FIG. 1. A realization of a uniformly mixed ice–water oblate spheroid in two orthogonal planes (x–y and y–z planes) for a water fraction of 0.3.

To find solutions to the large set of simultaneous linear equations obtained from the integral equation, an iterative procedure based on the conjugate gradient (CG) method is employed; the fast Fourier transform (FFT) is then used to compute the summation that appears in the form of a convolution. It has been demonstrated that the CGFFT numerical procedure not only has great flexibility with respect to the particle shape and materials composing the particle, but is also numerically efficient. Details of the theory can be found in the appendix.

3. Compositions of mixed-phase particles

A wide range of nonspherical hydrometeor shapes—such as discs, plates, columns, and needles that are most frequently present in the atmosphere—can be well approximated by oblate and prolate spheroids by changing the axial ratios. It is therefore reasonable to use spheroids in modeling nonspherical mixed-phase hydrometeors to check the validity of the effective dielectric constant. Melting snowflakes can be described as a mixture of snow and water, that is, two-component mixtures, though snow itself is composed of air and ice. For simplicity but without losing generality, we assume that the mixed-phase spheroids are composed of ice and water that are randomly mixed within the particle. It is worth mentioning that our study focuses on the examination of effective dielectric constants of nonspherical mixing particles rather than on modeling mixed-phase hydrometeors. Thus, it is sufficient for our purposes here to use uniformly mixed ice–water spheroids to describe nonspherical mixtures. Shown in Fig. 1 is an example of realization of an oblate spheroid projected onto two mutually perpendicular cross sections (x–y and x–z planes). The particle is composed of 128 cells along the x and y directions and 64 cells along the z axis, leading to an axial ratio of 0.5. The dark and light areas represent water and ice, respectively. The minimum size of any element (ice and water) is chosen to be at least $4 \times 4 \times 4$ cells in size to better satisfy the boundary conditions at the interfaces of ice and water. However, this requirement is not enforced near the particle boundary because higher-resolution grids are needed to precisely prescribe the surface contour.

To construct a uniformly mixed ice–water spheroid, the cells that make up the particle are first identified from a collection of $n_x \times n_y \times n_z$ grids along the x, y, and z directions where the number of grid elements along each direction is proportional to the particle size. If the number of cells (water and ice) is denoted by N_T, the number of water cells N_W for a given water fraction f_W is the product of f_W and N_T. A random generator is used to find N_W water cells from the pool of N_T cells. As noted above, the particle is composed of clusters of $4 \times 4 \times 4$ cells, which are not allowed to overlap. The ice–water mixture shown in Fig. 1 is constructed with a water fraction of 0.3 in accordance with the procedure described above. Several other realizations of ice–water particles are displayed in Fig. 2 with axial ratios of 0.5 and 0.125 (oblate spheroids in Figs. 2a and 2b, respectively) as well as 2 and 8 (prolate spheroids in Figs. 2c and 2d, respectively) for a fixed water fraction of 0.3. These are described, respectively, by collections of $128 \times 128 \times 64$, $256 \times 256 \times 32$, $64 \times 64 \times 128$, and

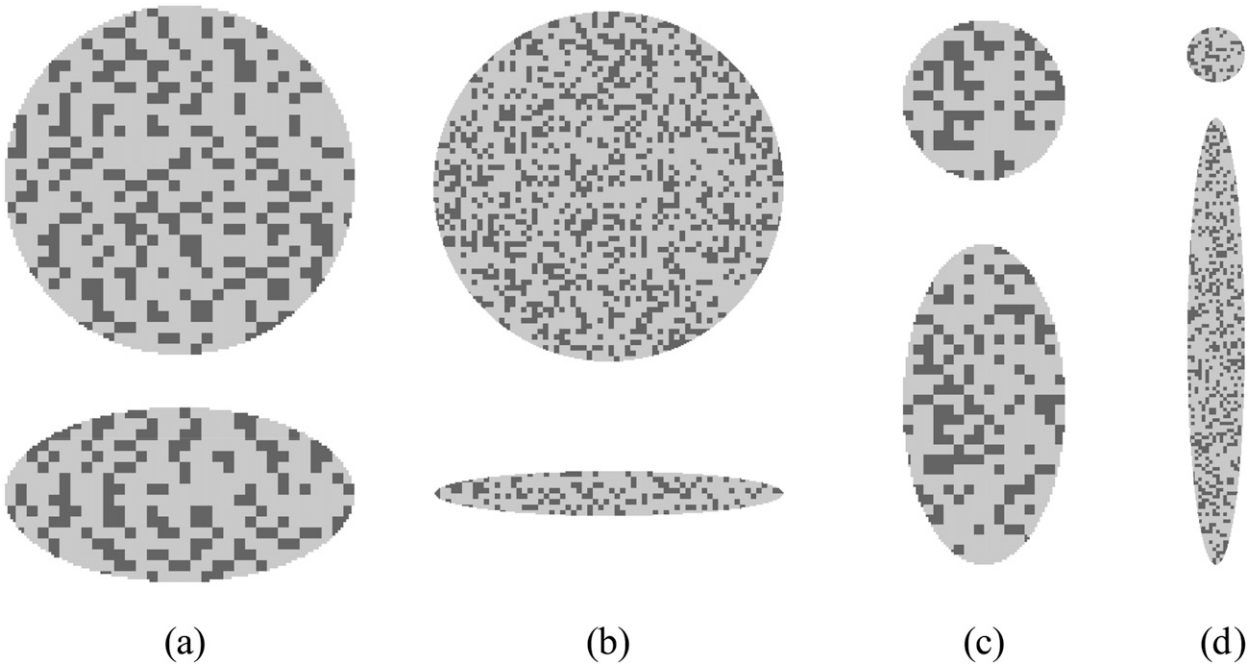

FIG. 2. Realizations of mixed-phased oblate and prolate spheroids in two orthogonal planes. (top) The top view and (bottom) the side view. (a),(b) Oblate spheroids described respectively by a collection of $128 \times 128 \times 64$ and $256 \times 256 \times 32$ equal cells that yield axial ratios of 0.5 and 0.125. (c),(d) Prolate spheroids consisting, respectively, of a collection of $64 \times 64 \times 128$ and $64 \times 64 \times 512$ equal cells that yield axial ratios of 2 and 8.

$64 \times 64 \times 512$ equal-volume cells. With such high-resolution models ($\sim 128^3$ cells), it can be seen that the particle shape and structure can be captured accurately.

4. Verification of effective dielectric constant

The validity of the derived effective dielectric constant for a nonspherical mixed-phase particle can be checked by comparing the scattering and polarimetric parameters of a mixed-phase (ice water) spheroid obtained from the CGFFT to those computed from the T-matrix method for a homogeneous particle with the same geometry as that of the mixed-phase particle with an effective dielectric constant derived from the internal field of the mixed-phase particle. These procedures can be illustrated schematically by the chart shown in Fig. 3, where $\varepsilon_{\mathrm{eff}}$ is the effective dielectric constant derived from the average internal fields of the particle realizations using the CGFFT numerical scheme. Scattering parameters, such as the phase function $[P(\Theta, \Phi)]$ and backscattering, scattering, and extinction coefficients (σ_b, σ_s, and σ_e), are compared between the CGFFT direct computations and T-matrix results. The degree of agreement between the two sets of results provides a criterion by which to judge the effective dielectric constant formulation.

For the sake of brevity, computations of scattering parameters as well as derivations of effective dielectric constants are made only at a frequency of 35 GHz (Ka band) with a fixed water fraction chosen as 0.3. The dielectric constants of ice and water are computed at 0°C using the regression equations reported by Ray (1972). The scattering geometry of a spheroid is provided in Fig. 4, where the incident wave propagates along the z direction while the parallel and perpendicular polarizations of the incident electric fields are along the x and y axes, respectively. The symmetry axis of the spheroid is described by a zenith angle of θ and azimuth angle of φ with respect to the x axis. The equatorial semidiameter and the radius at the poles of the spheroid are denoted by a and b, respectively.

Figure 5 shows the results of the normalized angular scattering intensity as a function of the scattering angle from the CGFFT and T-matrix computations for an ice–water mixed spheroid with size parameter x ($x = 2\pi r/\lambda$, where r is the equivalent-volume radius and λ is the wavelength) of 1 and axial ratio of 0.5. The particle is oriented at angles of $\theta = 45°$ and $\varphi = 45°$. The normalized angular scattering intensity, which is similar to the scattering phase function, is the electric field scattering intensity normalized by the cross-sectional area of the particle equivalent-volume sphere, that is, πr^2.

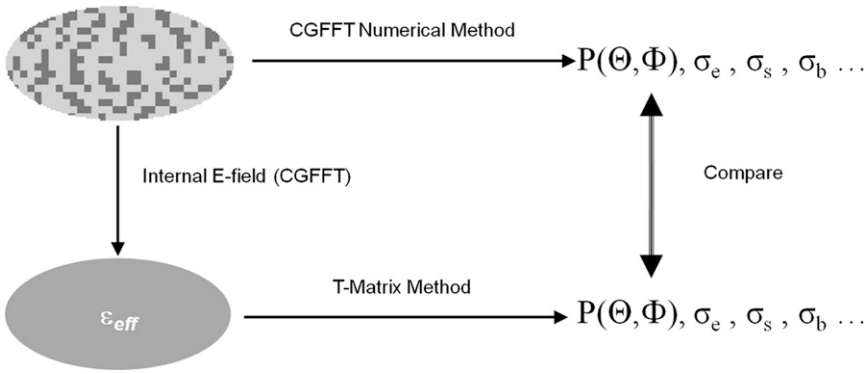

FIG. 3. Schematic diagram illustrating the validation procedure used to assess the accuracy of the effective dielectric constants of nonspherical particles.

The scattering angle is defined as the angle between the incident wave direction (Z axis) and the scattering direction in the X–Z plane. Since parallel polarization of the incident wave is assumed, the copolarized scattering intensity, shown in the left panel of Fig. 5, is equal to the scattered field along the θ direction while the cross-polarized (perpendicular) scattering intensity is equal to the scattered field along the φ direction, as depicted in the right panel of Fig. 5. Among these results are the CGFFT computations from three particle realizations, in which the ice–water cells are replaced by a new random configuration while keeping the water fraction as well as the shape, size, and orientation of the particle fixed. The T-matrix results, denoted by TM, are computed from the homogeneous particle with the same geometry as that of the mixed-phase particle using the CGFFT-derived effective dielectric constant. Note that the effective dielectric constant is taken as the mean of the results derived from the three particle realizations. The results in Fig. 5 show that there is a fairly good agreement between the CGFFT direct computations and the T-matrix results. The agreement is particularly good for the copolarized scattered field. The cross-polarized scattering results generally yield good agreement, but the CGFFT results show fluctuations from one particle realization to next around the scattering angle of 120°. Nevertheless, the generally good agreement between the CGFFT computations from the mixed-phase spheroids and the T matrix from the uniform spheroids confirms the utility of the effective dielectric constant for nonspherical particles.

It is well known that the T-matrix approach is very effective in computing the scattering properties of spheroids. However, the solutions tend to diverge for highly eccentric spheroids, that is, those with small or large axial ratios. To ensure the accuracy of the T-matrix solutions, calculations of the scattering parameters (of the homogeneous particles with an effective dielectric constant) are performed using both the CGFFT and T-matrix methods. In principle, the results from the CGFFT and T matrix should be identical and any significant differences likely indicate a possible divergence of the T-matrix solution. As shown in Fig. 5, the scattering intensities obtained from the CGFFT for the uniform particle, notated by CGFFT (uniform), agree well with those from the T matrix. In addition, the results of the T matrix using an effective dielectric constant derived from the internal fields from a smaller-sized particle ($x = 0.5$) and denoted by TM* is included and should be compared with the standard result (TM) where the effective dielectric

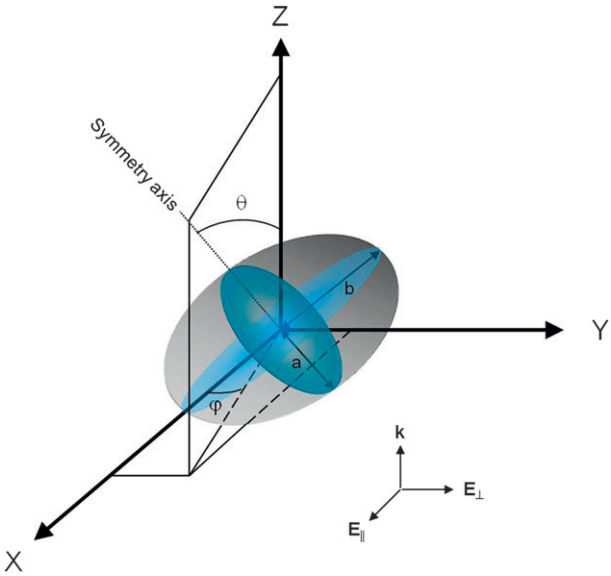

FIG. 4. Scattering geometry of a nonspherical particle with wave propagation vector (**k**) along the Z axis and the parallel and perpendicular polarizations of the incident wave along the X and Y axes, respectively.

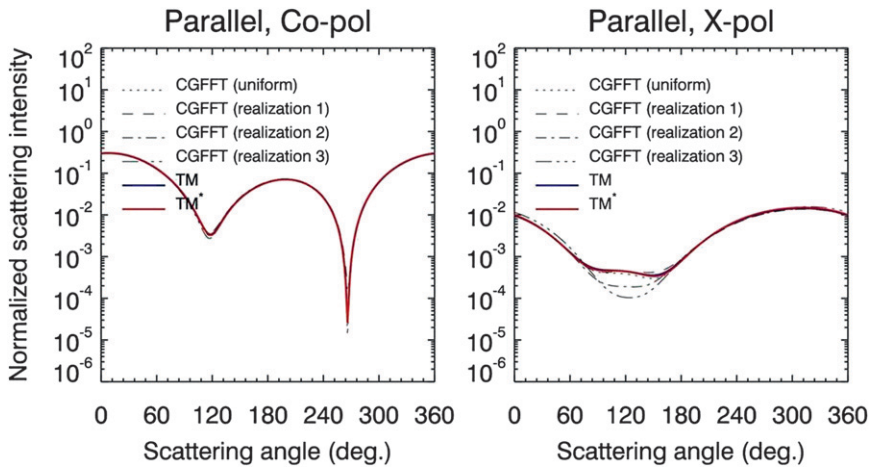

FIG. 5. Comparisons of normalized scattering intensities computed from the CGFFT for three oblate spheroid realizations with aspect ratio of 0.5 with the T-matrix results for the same particle shapes using the mean effective dielectric constants obtained from the CGFFT internal fields over several particle realizations. All the computations are made at a water fraction of 0.3 and particle size parameter of 1 as the spheroids are oriented at $\theta = 45°$ and $\varphi = 45°$. Labels TM and TM* refer to the results of the T-matrix computations using the effective dielectric constants derived for particle size parameters of 1 and 0.5, respectively. The CGFFT results that are computed from a uniform particle of mean effective dielectric constant are also included in the plots. The copolar and cross-polar angular scattering intensities are given in the left and right panels for the parallel-polarized incident wave.

constant is derived from the internal fields of a particle with size parameter $x = 1$. It is apparent that the results of TM and TM* are nearly indistinguishable, suggesting that the effective dielectric constants are to a great extent independent of particle sizes at which the effective dielectric constant is derived. This is an important feature in assessing the utility of the effective dielectric constant approach.

Comparisons of the means of the normalized copolarized scattering intensities over five particle realizations are made in Fig. 6 between the CGFFT direct computations (CGFFT) of ice–water oblate mixtures with axial ratio of 0.5 and the T-matrix results (TM) of uniform oblate spheroids with $\varepsilon_{\mathrm{eff}}$ as the particle size parameter varies from 0.1 to 4. The particles are oriented so that $\theta = 45°$ and $\varphi = 45°$. As in Fig. 5, the T-matrix results with the effective dielectric constant derived at $x = 0.5$ (TM*) are also plotted. Generally there is a reasonably good agreement among the scattering results of CGFFT, TM, and TM*. Not only does this reveal the validity of effective dielectric constants in the scattering computations for various particle sizes, but it also indicates that the scattering parameters of mixed-phase particles can be reproduced by the T matrix from uniform particles with an effective dielectric constant derived at a fixed particle size. The same conclusions can be drawn from similar computations but with different axial ratios and orientations of spheroids (not shown). It should be noted that the discrepancies between the scattering results from the CGFFT and T matrix (both TM and TM*) tend to become greater as the particle size increases. This is likely due to resonance effects (or Mie effects), that is, scattering intensities at larger particles that change rapidly with small variations in particle size, orientation, and composition.

As noted earlier, effective dielectric constant can be obtained using mixing formulas. Although a number of mixing formulas are available, their results vary to a great degree when water is one of the components in the mixture. Furthermore, it is physically unclear as to how to select among these various formulas (Meneghini and Liao 1996). Many of these mixing formulas, such as the Maxwell Garnett and Bruggeman mixing formulas, are derived from uniform mixtures in which mixing ratios are constant throughout the particles. To see how their scattering results compare with those from direct computations from specific particle realizations, shown in Fig. 7 are comparisons of the normalized scattering intensities between the CGFFT computations of ice–water oblate mixtures with axial ratio of 0.5 and the T-matrix results of uniform oblate spheroids with $\varepsilon_{\mathrm{eff}}$ derived from the Maxwell Garnett and Bruggeman's mixing formulas. Notations of $\mathrm{MG_{wi}}$ and $\mathrm{MG_{iw}}$ denote the results from the Maxwell Garnett equations, where $\mathrm{MG_{wi}}$ represents the case in which water is treated as matrix and ice as inclusion, and where $\mathrm{MG_{iw}}$ represents

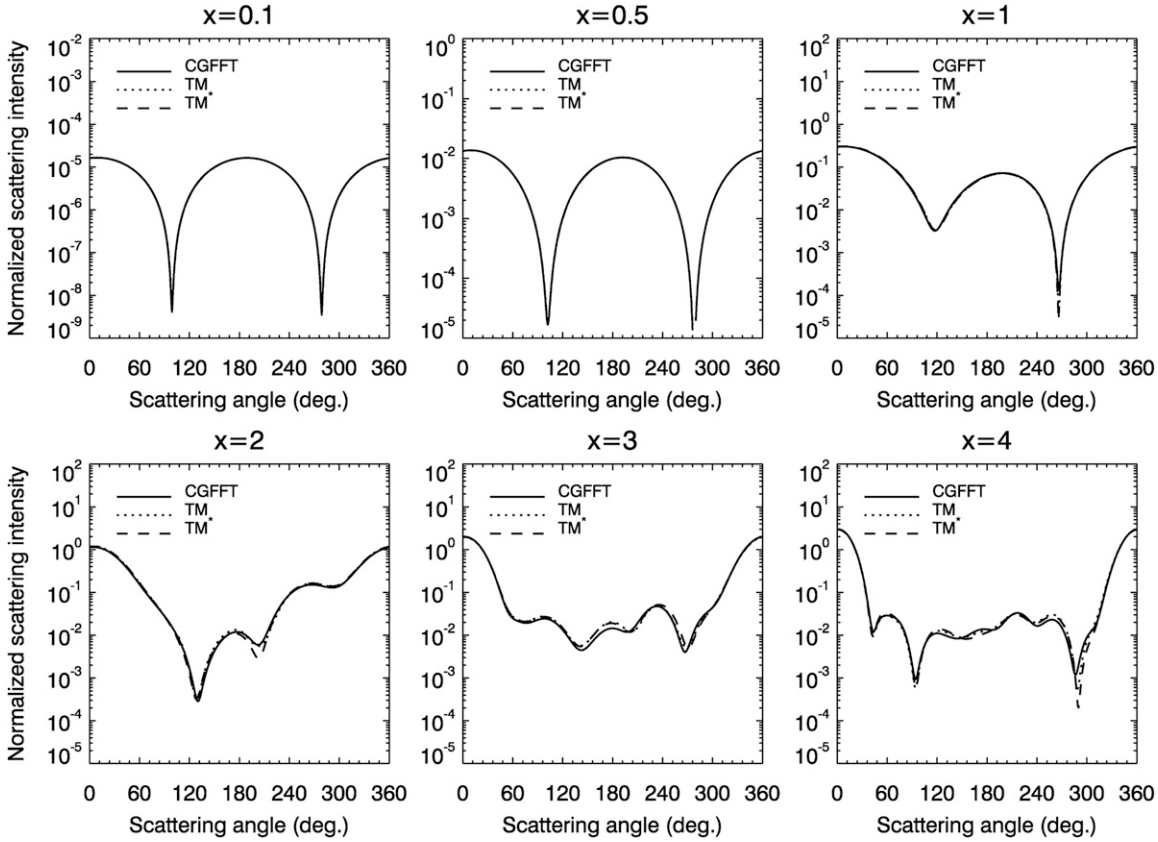

FIG. 6. Comparisons of the mean normalized scattering intensities between the CGFFT direct computations (CGFFT) of ice–water oblate mixtures with axial ratio of 0.5 and TM of uniform oblate spheroids using effective dielectric constants derived from the particle internal fields of 5 particle random realizations. All the computations are made as the spheroids are oriented at $\theta = 45°$ and $\varphi = 45°$ and particle size parameters (x) vary from (top left) 0.1 to (bottom right) 4. TM* represents the T-matrix results with the effective dielectric constant derived at $x = 0.5$.

the case in which the roles of water and ice are reversed, that is, ice as matrix and water as inclusion. As in Fig. 6, the scattering intensities are the mean of the results from five particle realizations. Computations are carried out as the spheroids are oriented at $\theta = 45°$ and $\varphi = 45°$, and particle size parameters vary from 0.1 to 4. It is evident that the degree of agreement with the CGFFT differs among the mixing formulas even though they all produce similar scattering patterns as that from the CGFFT. To quantify these differences, a relative error (δ) of the various formulations with respect to the CGFFT direct computation is defined as

$$\delta = \frac{1}{N}\sum_{i=1}^{N}\frac{|F_M(\theta_i) - F_{\mathrm{CGFFT}}(\theta_i)|}{F_{\mathrm{CGFFT}}(\theta_i)} \times 100, \qquad (4)$$

where $F_{\mathrm{CGFFT}}(\theta)$ and F_M are the normalized angular scattering intensities obtained by the direct CGFFT computations and the T matrix with $\varepsilon_{\mathrm{eff}}$, respectively. The N is the total number of scattering angles used in the computations over the range from 0° to 360°. Table 1 summarizes the results of the relative errors of the T-matrix computations from Figs. 6 and 7 with $\varepsilon_{\mathrm{eff}}$ derived from the particle internal fields (TM and TM*) and the mixing formulas (Maxwell Garnett and Bruggeman). Note that since the scattering computations are made at 5 particle realizations, the errors given in Table 1 are the averaged results from these realizations. The results clearly show that the $\mathrm{MG_{wi}}$ departs greatly from the CGFFT for small to moderate particles ($x \leq 2$) and tends to agree better with the CGFFT results for large particles ($x > 2$). In contrast to the $\mathrm{MG_{wi}}$, the $\mathrm{MG_{iw}}$ has small errors for small particles ($x \leq 1$) and large errors for the big particles ($x \geq 2$). The results from the Bruggeman mixing formula exhibit fairly good agreement with the CGFFT direct computations. However, the best agreement occurs for the results of the TM and TM*. It is important to note that these comparisons were done only for a single frequency and water fraction; a separate study would be needed to draw more

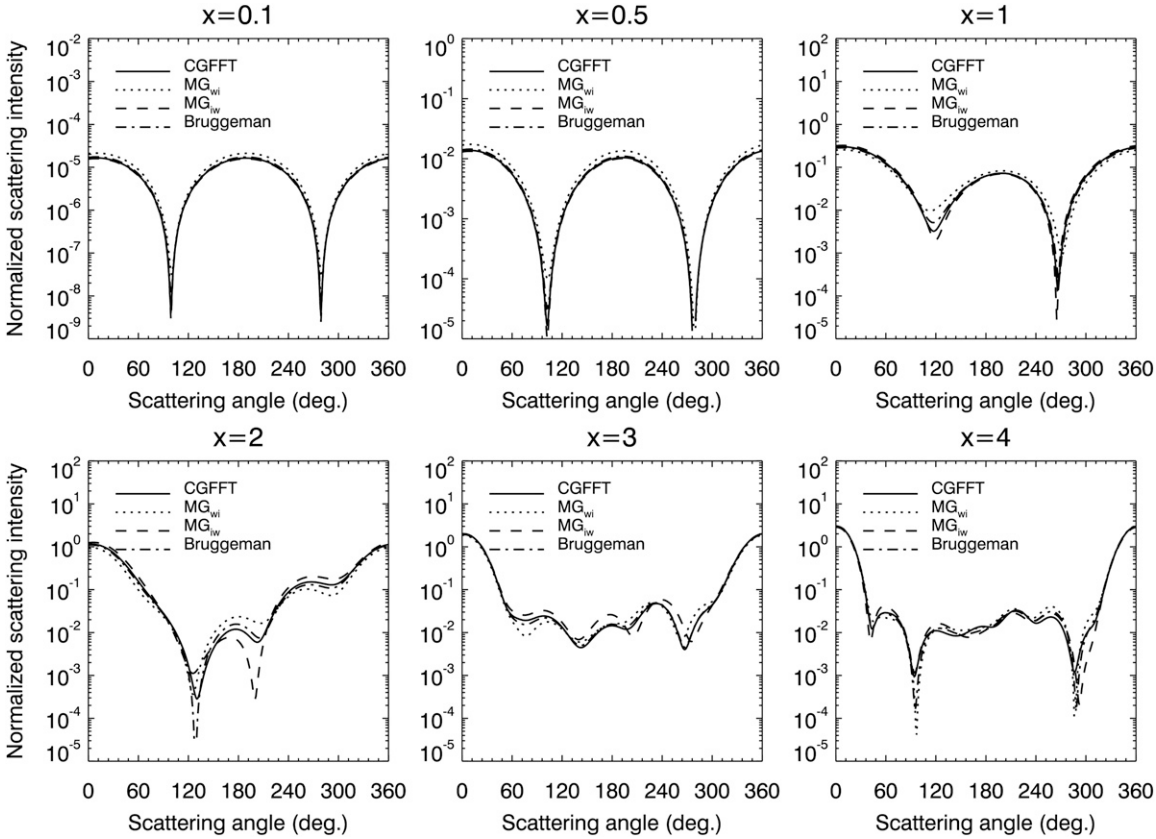

FIG. 7. As in Fig. 6, but using effective dielectric constants obtained from the Maxwell Garnett and Bruggeman mixing formulas. Notations of MG_{wi} and MG_{iw} stand for two Maxwell Garnett results, one in which water is treated as the matrix with ice inclusions (MG_{wi}), and the other in which the roles of water and ice are reversed, i.e., ice as matrix and water as inclusion (MG_{iw}).

general conclusions as to the suitability of any of the standard dielectric formulas to nonspherical mixed-phase particles.

Up to this point the paper's emphasis is on the existence and validity of the effective dielectric constant for nonspherical mixed-phase particles. The effective dielectric constant, however, would have limited applicability if it depended on the particle size or geometry or particular orientation, apart from the fractional water content. To check the independence on particle size and geometry, we use below the complex refractive index, defined as square root of dielectric constant, as it is frequently used in the radar and radiometer literature to describe the scattering properties of hydrometeors. This quantity will be used to check the variations in the dielectric properties of ice–water mixtures for different particle geometries. Figure 8 shows the real (blue) and imaginary (red) parts of complex refractive indexes derived from oblate and prolate spheroids as well as spheres. For a fixed size parameter, results are displayed for the various refractive indices derived from different particle realizations with various orientations and axial ratios. The solid lines represent the mean values of the data. The results show that greater variations occur for larger particles; moreover, this variation is more pronounced for prolate spheroids than for spheres or oblate spheroids. The mean values, however, remain relatively stable with changes in size, shape, and orientation—properties that we would require from the perspective of practical applications, that is, that the effective dielectric

TABLE 1. Relative errors (%) of normalized angular scattering intensities of Figs. 6 and 7, computed by T matrix using effective dielectric constants derived from particle internal fields and mixing formulas, as compared with the CGFFT direct computations. Here, x refers to the particle size parameter.

x	TM	TM*	MG_{wi}	MG_{iw}	Bruggeman
0.1	1	1	88	2	4
0.5	1	1	64	1	4
1	3	4	143	4	15
2	4	5	130	216	8
3	6	12	21	61	6
4	6	15	31	43	22

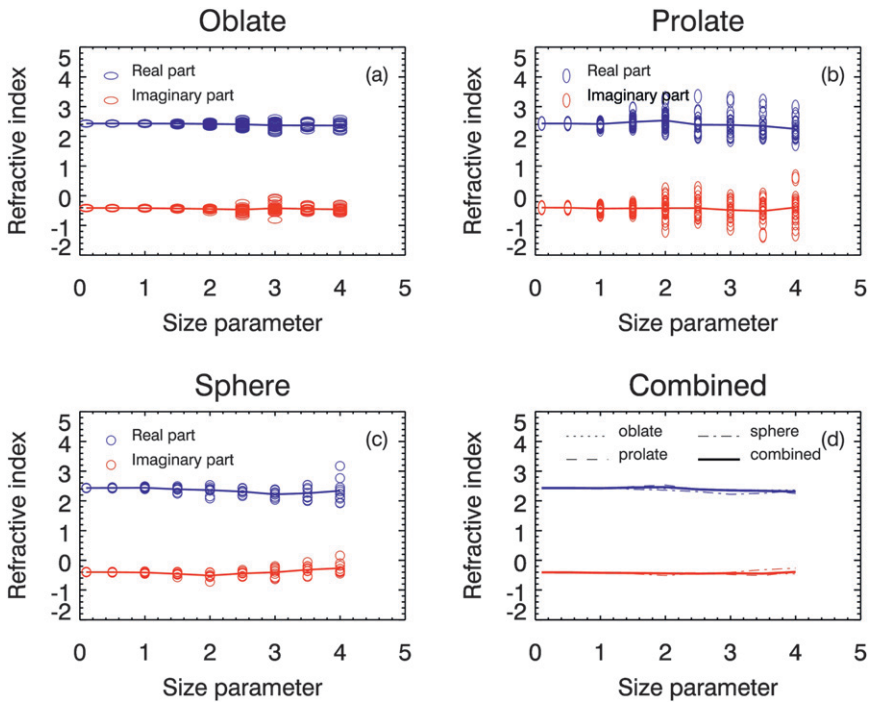

FIG. 8. Complex refractive indices, defined as the square root of the dielectric constant, computed from mixed-phase particle realizations of (c) spheres and (a) oblate and (b) prolate spheroids as a function of the particle size parameter. Real and imaginary parts of the complex refractive indices are given by the blue and red circles, respectively, with solid lines representing the mean value. For oblate and prolate spheroids the data points at a fixed size correspond to the results computed from different aspect ratios and orientations of the particles but with the same sizes, i.e., equivalent volumes. The results include computations made for several particle realizations for each particle size, shape, and orientation. (d) Mean values of the real (blue) and imaginary (red) parts of the complex refractive index for oblate, prolate, and spherical particles and their averaged results (combined).

constant is independent of the particle geometry. To present these results in a different way, the complex refractive indexes are plotted, as shown in Fig. 9, in the plane of complex refractive index in which the real part of refractive index is along the abscissa and the imaginary part along the ordinate. As in Fig. 8, the data are broken down into three categories according to particle shape (Figs. 9a–c). The merged data are shown in Fig. 9d. The results for different particle sizes are depicted by the size of the data ''point'' using the scale shown on the right-hand size of the plot. The means are represented by the intersections of the solid vertical and horizontal lines with their values given in the brackets. The results show that large particles (represented by the big circles) are responsible for most of the variation from realization to realization. Moreover, the prolate spheroids show larger fluctuations than either the oblates or spheres. This is consistent with the results shown in Fig. 8. Despite these variations, the mean values are nearly invariant with respect to particle shape or size. As shown in Figs. 8 and 9, the fluctuations in the complex refractive index are much smaller when the particle size is small. This suggests that the means of the refractive indices (or effective dielectric constants) could be accurately computed at small particle sizes and without the need to average many realizations to achieve stability in the mean. The CGFFT at small particle sizes has a computational advantage over large particles because the time to convergence of the results for small particles is significantly shorter than those for large particles. This, in conjunction with small number of the realizations needed, leads a dramatic reduction in CPU time if the effective dielectric constants are derived at small sizes. In view of the variability of the complex refractive indexes shown in Figs. 8 and 9, it is recommended that the effective dielectric constants be computed at particle size parameters of 0.5 or smaller. For reference the means of the complex refractive indexes derived at $x = 0.5$ are also plotted in Fig. 9, which are the intersections of two orthogonal dashed lines. The results show that

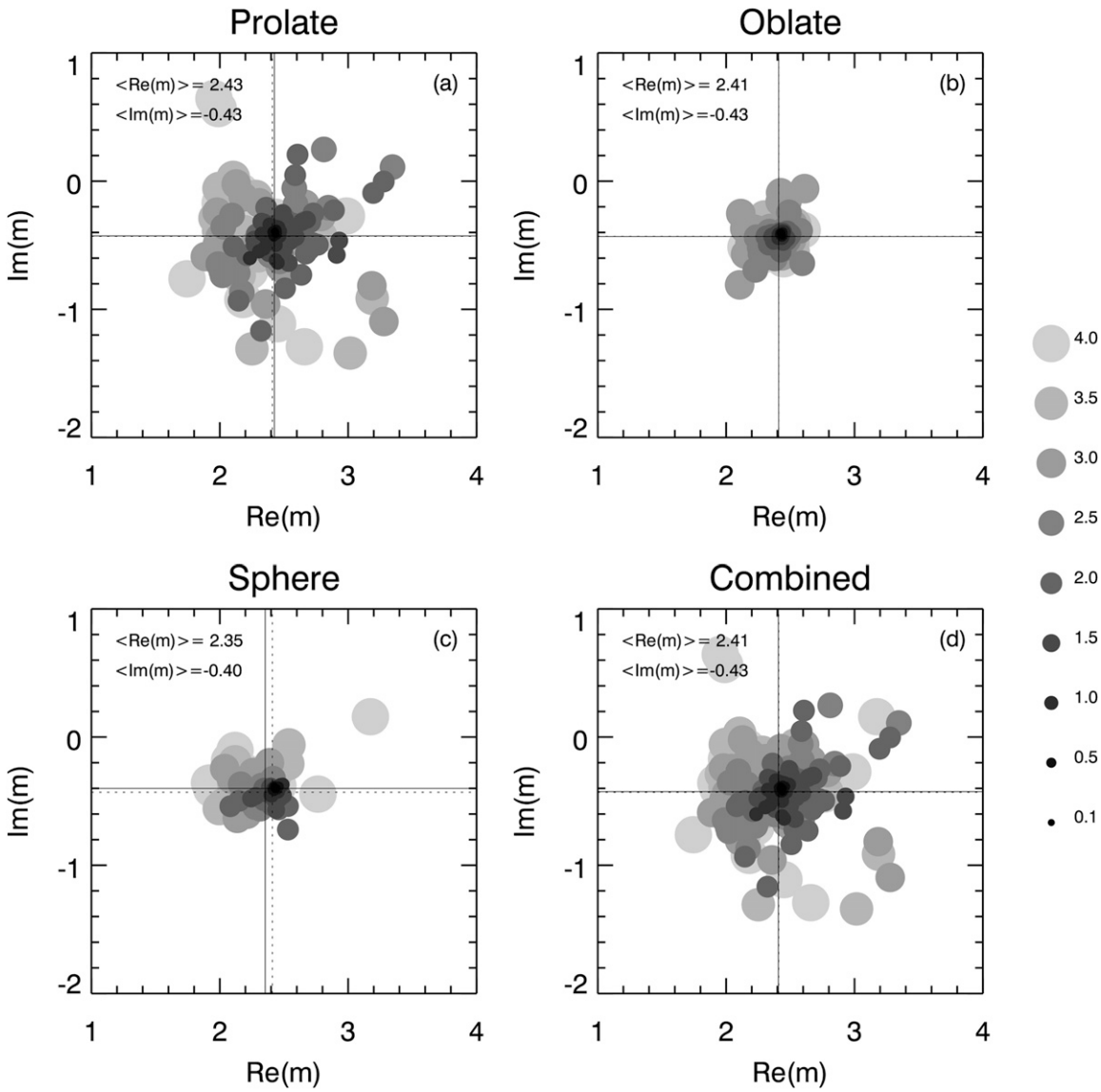

FIG. 9. Scatterplots of the derived complex refractive indices (m) in the complex plane with the real part (Re) along the abscissa and imaginary part along the ordinate. The size of each data point is proportional to the particle size parameters as shown by the scale on the right-hand side. The mean values of the real and imaginary parts are given in each panel and are also indicated by the intersection of the vertical and horizontal solid lines. The intersection of the dashed lines corresponds to the mean complex refractive index that is computed exclusively from the particles with a size parameter of 0.5. The data are broken down into results from (a) oblate spheroids, (b) prolate spheroids, (c) spheres, and (d) combined.

the mean average effective refractive index derived for $x = 0.5$ differs little from the results derived from the average effective refractive index of larger particles.

To see if radar and radiometer scattering parameters can be reproduced with use of effective dielectric constants, comparisons of several scattering parameters are shown in Fig. 10 between the direct (CGFFT) computations from mixed-phase particle realizations and the T-matrix computations using the effective dielectric constant. For these computations the particle size parameter ranges from 0.1 to 4. The computations are carried out for oblate and prolate spheroids with axial ratios varying from 0.125 to 8 as well as for spheres at each particle size. Results from two particle orientations are shown: $(\theta, \varphi) = (0, 0)$ and $(\theta, \varphi) = (45°, 45°)$. The scattering parameters included in the comparisons are the backscattering ($\sigma_{b,\mathrm{hh}}$), scattering ($\sigma_{s,\mathrm{hh}}$), and extinction ($\sigma_{e,\mathrm{hh}}$) coefficients, asymmetry factor (g_{hh}), $|\mathrm{Re}(f_{\mathrm{hh}} - f_{\mathrm{vv}})|$, and linear depolarization ratio [LDR; defined as $10 \log_{10}(\sigma_{b,\mathrm{hv}}/\sigma_{b,\mathrm{hh}})$]. In the notation "hh,"

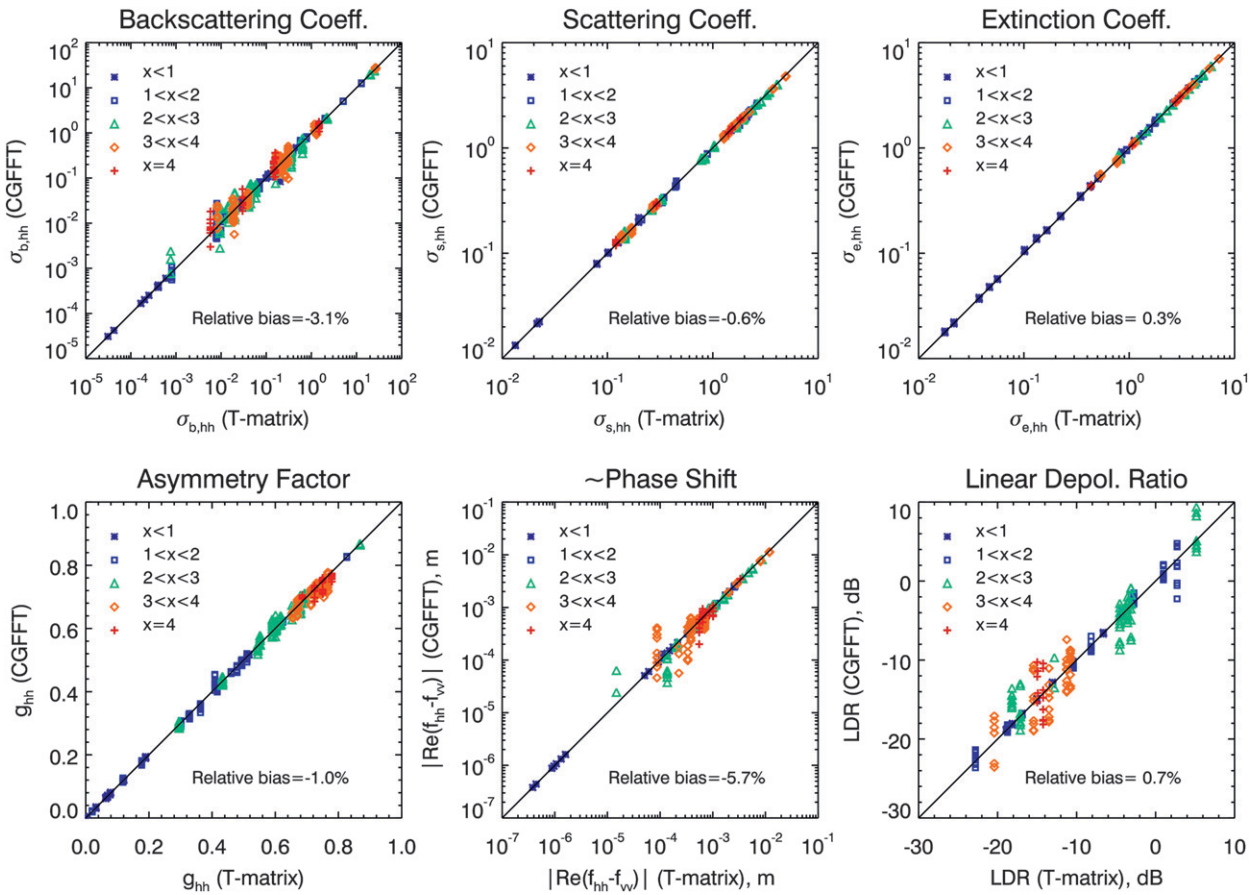

FIG. 10. Comparisons of scattering parameters computed from the CGFFT direct computations and T matrix for uniform particles with effective dielectric constants. Particle shapes include spheres as well as oblate and prolate spheroids. The scattering parameters shown are backscattering coefficient (σ_b), scattering coefficient (σ_s), extinction coefficient (σ_e), asymmetry factor (g), absolute value of real part of the difference of scattering amplitudes between horizontal and vertical polarizations ($|\mathrm{Re}(f_{\mathrm{hh}} - f_{\mathrm{vv}})|$) (which is proportional to the phase shift of propagation between horizontal and vertical polarizations), and LDR. The subscripts hh and vv denote the copolarized returns for horizontal and vertical polarizations, respectively.

"hv," and so on, the first subscript denotes the polarization state of the incident wave while the second denotes the polarization of the scattered field. The quantity f is the forward-scattering amplitude while $|\mathrm{Re}(f_{\mathrm{hh}} - f_{\mathrm{vv}})|$ represents the absolute value of the real part of the difference of forward-scattering amplitudes between horizontal and vertical polarizations, and is proportional to the propagation phase shift. For $(\theta, \varphi) = (0, 0)$ where the symmetry axis of the particle is aligned along the propagation direction of the incident wave, f_{hh} and f_{vv} are identical, and therefore the phase shift $[|\mathrm{Re}(f_{\mathrm{hh}} - f_{\mathrm{vv}})|]$ is 0. Moreover, for this geometry, there is no cross-polarized backscattering, that is, $\sigma_{b,\mathrm{hv}} = 0$, leading to LDR equal to negative infinity. These results also hold for spheres. As such, the results for LDR and $|\mathrm{Re}(f_{\mathrm{hh}} - f_{\mathrm{vv}})|$ for the case of $(\theta, \varphi) = (0, 0)$ are not included in Fig. 10. The relative biases of the scattering parameters obtained from the homogeneous and mixed-phase particles are also given in Fig. 10. The relative bias is defined as

$$\text{relative bias} = \frac{1}{N}\sum_{i=1}^{N}\frac{S_{i,\mathrm{TM}} - S_{i,\mathrm{CGFFT}}}{S_{i,\mathrm{CGFFT}}} \times 100\%, \qquad (5)$$

where S represents the scattering parameter (σ_b, σ_e, LDR ...), N is the total number of particle realizations used in computations, and subscripts TM and CGFFT refer to the T-matrix (homogeneous particles) and CGFFT direct computations (mixed-phase particles). There are about 630 realizations, that is, $N \approx 630$, covering particle size parameters from 0.1 to 4, and axial ratios from 0.125 to 8. It is not difficult to find, as shown in Fig. 10, that there exist high correlations between the CGFFT and the T-matrix results for each of the scattering parameters. The relative biases remain fairly small (less than ±1% for most of the scattering

parameters) with the largest biases of −3.1% for the backscattering coefficient and −5.7% for $|\mathrm{Re}(f_{hh} - f_{vv})|$. In short, the good agreement between the scattering parameters for mixed-phase particles and homogeneous particles with an effective dielectric constant implies that the use of an effective dielectric constant formulation to derive radar and radiometer co- and cross-polarized scattering parameters is efficient and sufficiently accurate if the hydrometeors can be modeled as spheroids.

5. Summary and remarks

Validation of the procedure to obtain an effective dielectric constant for nonspherical random mixtures of ice–water particles has been carried out by comparing co- and cross-polarized scattering properties, such as angular scattering intensity, backscattering, scattering and extinction coefficients, phase shift, and LDR, from realizations of high-resolution mixed-phase particle models with those from a homogeneous particle with dielectric constant $\varepsilon_{\mathrm{eff}}$. This is accomplished by modeling nonspherical particles as oblate and prolate spheroids and by comparing the scattering parameters of the mixed-phase oblate and prolate spheroids obtained from the CGFFT to those computed from the T matrix for a homogeneous particle with the same geometry as that of the mixed-phase particle (such as size, shape, and orientation) with an effective dielectric constant derived from the internal fields of the ice–water particle. The accuracy of the effective dielectric constant is judged by whether the scattering parameters of interest can accurately reproduce those of the direction computations, that is, the CGFFT results. Analysis of the results indicates that the effective dielectric constant of ice–water mixed-phase spheroids is sufficiently accurate to be used to compute the scattering properties of spheroids up to size parameters of approximately 4. Although the paper has shown comparisons for a fixed frequency and fractional water, computations at other values of frequencies and water fractions of these parameters indicate similar good agreement. These results imply that scattering computations for mixed-phase particles by complex and time-consuming numerical methods can be replaced by fast analytical solutions using homogenous particles of the same geometry with an effective dielectric constant. This is particularly true for the typical radar or radiometer viewing geometry over a large field of view where the variations in the scattered fields from individual particles will tend to cancel out.

The utility of $\varepsilon_{\mathrm{eff}}$ has been examined through comparisons of the complex refractive indices derived from a class of particles for which the water fractions are fixed but the sizes, shapes, and orientations vary. It is concluded that the means of the complex refractive indices are nearly unchanged for different particle sizes, shapes, and orientations as long as the water fraction is fixed. It is also found that the variability in the complex refractive indices from large particle realizations is larger than from small particles even though the mean remains approximately the same. Because of this, it is suggested that the effective dielectric constants should be computed at small particle sizes, with a particle size parameter of 0.5 or smaller. Our findings of this study indicate that the effective dielectric constant, once obtained, can be applied to a range of particles sizes, shapes, and orientations for a fixed fractional water content. The use of the effective dielectric constant may greatly reduce the complexity and computational time of the scattering calculations. It should be noted, moreover, that although results in this paper are presented only for a frequency of 35 GHz and a water fraction of 0.3, the findings seem to be applicable to other frequencies and water fractions based on our computations made at different frequencies and water fractions.

While the effective dielectric constant approach provides a simple and accurate means to compute scattering parameters of mixed-phase particles, successful simulations of radar and radiometer polarimetric scattering parameters require appropriate hydrometeor melting models, such as shapes, orientations, and more importantly melting processes that determine how the melted water is distributed within the particle. An investigation of these more general particle models with more accurate representations of the melted-water distribution will be next steps toward the development of a more complete and accurate melting layer scattering model in an attempt to improve the accuracy of precipitation estimates by the Global Precipitation Measurement (GPM) Dual-Frequency Precipitation Radar (DPR) and Microwave Imager (GMI).

Acknowledgments. This work is supported by Dr. R. Kakar of NASA headquarters under NASA's Precipitation Measurement Mission (PMM) Grant NNH06ZDA001N-PMM.

APPENDIX

The CG-FFT Method and Its Use for Computations of Scattering Parameters

a. The CG-FFT method

The electric field **E** in a dielectric medium can be expressed in terms of the potential vector **A** and the scalar potential ϕ as

$$\mathbf{E} = -\nabla\phi - \frac{\partial \mathbf{A}}{\partial t}, \tag{A1}$$

where $\mathbf{A}$ and ϕ yield

$$\nabla^2\mathbf{A}(\mathbf{r}) + k_0^2\mathbf{A}(\mathbf{r}) = -\mu_0\mathbf{J} \quad \text{and} \tag{A2}$$

$$\nabla^2\phi(\mathbf{r}) + k_0^2\phi(\mathbf{r}) = -\frac{\rho}{\varepsilon_0}, \tag{A3}$$

where $\mathbf{J}$ and ρ are the volume densities of the current and charge, respectively, and k_0 is the free-space propagation constant in consideration of the periodic time-dependent fields, in which an $\exp(i\omega t)$ time convention is assumed and suppressed.

Using the free-space Green's function $G(k_0R) = \exp(-jk_0R)/4\pi R$, $R = |\mathbf{r} - \mathbf{r}'|$, $\varphi(\mathbf{r})$ and $\mathbf{A}(\mathbf{r})$ can be derived to be

$$\varphi(\mathbf{r}) = \frac{1}{\varepsilon_0}\iiint_V \rho(\mathbf{r}')G(k_0, R)\,d\mathbf{r}' \quad \text{and} \tag{A4}$$

$$\mathbf{A}(\mathbf{r}) = \mu_0\iiint_V \mathbf{J}(\mathbf{r}')G(k_0, R)\,d\mathbf{r}', \tag{A5}$$

where $\mathbf{r}'$ and $\mathbf{r}$ are the coordinates for the source and observation points.

Let us consider a plane wave $\mathbf{E}^i$ incident on a dielectric particle. According to (A1), the electric field at any point of space is

$$\mathbf{E}(\mathbf{r}) = \mathbf{E}^i(\mathbf{r}) - j\omega\mathbf{A}(\mathbf{r}) - \nabla\phi(\mathbf{r}). \tag{A6}$$

Since there are no free charges in the space, the $\rho(\mathbf{r})$ and $\mathbf{J}(\mathbf{r})$ are

$$\rho(\mathbf{r}) = -\varepsilon_0\nabla\cdot\{[\overline{\overline{\varepsilon_\mathbf{r}}}(\mathbf{r}) - \overline{\overline{\mathbf{I}}}]\mathbf{E}(\mathbf{r})\} \quad \text{and} \tag{A7}$$

$$\mathbf{J}(\mathbf{r}) = j\omega\varepsilon_0[\overline{\overline{\varepsilon_\mathbf{r}}}(\mathbf{r}) - \overline{\overline{\mathbf{I}}}]\mathbf{E}(\mathbf{r}), \tag{A8}$$

where $\overline{\overline{\varepsilon_\mathbf{r}}}$ and $\overline{\overline{\mathbf{I}}}$ are the generalized complex tensor of the relative permittivity of the medium and the unit matrix, respectively. From the substitution of (A4) and (A5) into (A6) using (A7) and (A8), we obtain

$$\mathbf{E}(\mathbf{r}) = \mathbf{E}^i(\mathbf{r}) + \omega^2\mu_0\varepsilon_0\iiint_\infty G(k_0R)[\overline{\overline{\varepsilon_\mathbf{r}}}(\mathbf{r}') - \overline{\overline{\mathbf{I}}}]\mathbf{E}(\mathbf{r}')\,d\mathbf{r}' + \nabla\iiint_\infty G(k_0R)\nabla'\cdot\{[\overline{\overline{\varepsilon_\mathbf{r}}}(\mathbf{r}') - \overline{\overline{\mathbf{I}}}]\mathbf{E}(\mathbf{r}')\}\,d\mathbf{r}'. \tag{A9}$$

After applying integration by parts to the last term of (A9), we have

$$\begin{aligned}\mathbf{E}(\mathbf{r}) &= \mathbf{E}^i(\mathbf{r}) + \omega^2\mu_0\varepsilon_0\iiint_\infty G(k_0R)[\overline{\overline{\varepsilon_\mathbf{r}}}(\mathbf{r}') - \overline{\overline{\mathbf{I}}}]\mathbf{E}(\mathbf{r}')\,d\mathbf{r}' \\ &\quad + \iiint_\infty \nabla\nabla G(k_0R)[\overline{\overline{\varepsilon_\mathbf{r}}}(\mathbf{r}') - \overline{\overline{\mathbf{I}}}]\mathbf{E}(\mathbf{r}')\,d\mathbf{r}' \\ &= \mathbf{E}^i(\mathbf{r}) + \iiint_\infty \overline{\overline{\mathbf{G}}}(k_0R)\overline{\overline{\mathbf{X}}}(\mathbf{r}')\mathbf{E}(\mathbf{r}')\,d\mathbf{r}',\end{aligned} \tag{A10}$$

where

$$\overline{\overline{\mathbf{G}}}(k_0R) = (k_0^2\overline{\overline{\mathbf{I}}} + \nabla\nabla)G(k_0R) \quad \text{and} \tag{A11}$$

$$\overline{\overline{\mathbf{X}}}(r') = \overline{\overline{\varepsilon_\mathbf{r}}}(\mathbf{r}') - \overline{\overline{\mathbf{I}}}. \tag{A12}$$

From (A10) the scattered field is given by

$$\mathbf{E}^s(\mathbf{r}) = \iiint_{V_p} \overline{\overline{\mathbf{G}}}(k_0R)\overline{\overline{\mathbf{X}}}(\mathbf{r}')\mathbf{E}(\mathbf{r}')\,d\mathbf{r}', \tag{A13}$$

where V_p is the volume of the particle; when outside the particle, $\overline{\overline{\mathbf{X}}}(\mathbf{r}') = 0$.

To employ the FFT technique discussed below, the integration volume V_p is replaced by V, where V is selected to be orthogonal and enclose the total particle. Then V is divided into $m_1 \times m_2 \times m_3$ identical orthorhombic cells with volume $\Delta v = \Delta x\Delta y\Delta z$, which is small enough so that every component of the field is approximately constant within Δv. Using center points (x_i, y_j, z_k) of Δv, where $i = 1, \ldots, m_1$, $j = 1, \ldots, m_2$ and $k = 1, \ldots, m_3$, to represent each component, and expanding (A13), we have

$$E_p(i,j,k) = \mathbf{E}_p^i(i,j,k) + \sum_{i'=1}^{m_1}\sum_{j'=1}^{m_2}\sum_{k'=1}^{m_3}\sum_q g_{\mathrm{pq}}(i-i', j-j', k-k')\cdot\sum_t \varepsilon_{\mathrm{qt}}(i',j',k')E_t(i',j',k'), \tag{A14}$$

where $p = x, y, z$ and the summation for q and t is x, y, z. The g_{pq} denotes the product of the elements of the matrix $\overline{\overline{\mathbf{G}}}(k_0R)$ and Δv, while $\varepsilon_{\mathrm{qt}}$ denotes the (qt)th elements of $\overline{\overline{\mathbf{X}}}(\mathbf{r}')$. Equation (A14) can be written as a set of $3M$ unknowns $\mathbf{E}(x_i, y_j, z_k)$:

$$\mathbf{AX} = \mathbf{B}, \tag{A15}$$

where $\mathbf{A}$ is the coefficient matrix of order $3M \times 3M$, $\mathbf{X}$ is the unknown matrix of order $3M \times 1$, consisting of the elements $E_p(i, j, k)$, and $\mathbf{B}$ is the excitation matrix of order

$3M \times 1$ composed of the elements $E_p^i(i,j,k)$. The conjugate gradient method, which is an iterative procedure, is employed to solve the set of $3M$ simultaneous linear equations in (A15). An $\tilde{\mathbf{A}}$ is chosen to be the transpose (t) of the complex conjugate (*) of $\mathbf{A}$, that is, $\tilde{\mathbf{A}} = (\mathbf{A}^*)^t$, so that $\tilde{\mathbf{A}}\mathbf{A}$ is Hermitian. This kind of iterative method does not stop until $\|\mathbf{B} - \mathbf{AX}\| \le \varepsilon$, where ε is some small number related to the accuracy of the solution. It is important to note that the multiple summations of (A14) are in the form of a convolution, and therefore it can be computed by the discrete convolution theory associated with the FFT. Letting $n_1 = 2m_1$, $n_2 = 2m_2$, and $n_3 = 2m_3$, the functions $G_{\mathrm{pq}}(i',j',k')$ and $P_q(i',j',k')$ with period of n_1, n_2, and n_3 for each dimension, respectively, are constructed below:

$$G_{\mathrm{pq}}(i+l_1, j+l_2, k+l_3) = \begin{cases} g_{\mathrm{pq}}(i,j,k), & -(m_1-1) \le i \le m_1 - 1 \\ & -(m_2-1) \le j \le m_2 - 1 \\ & -(m_3-1) \le k \le m_3 - 1 \\ 0, & i = -m_1 \quad \text{or} \quad j = -m_2 \quad \text{or} \quad k = -m_3 \end{cases}, \tag{A16}$$

where

$$l_1 = \begin{cases} 0, & i \ge 0 \\ n_1, & i < 0 \end{cases} \quad l_2 = \begin{cases} 0, & j \ge 0 \\ n_2, & j < 0 \end{cases} \quad l_3 = \begin{cases} 0, & k \ge 0 \\ n_3, & k < 0 \end{cases},$$

and

$$P_q(i,j,k) = \begin{cases} \varepsilon_{\mathrm{qt}}(i,j,k)E_t(i,j,k), & 0 \le i \le m_1 - 1 \\ & 0 \le j \le m_2 - 1 \\ & 0 \le k \le m_3 - 1 \\ 0, & m_1 \le i \le n_1 - 1 \quad \text{or} \quad m_2 \le j \le n_2 - 1 \quad \text{or} \quad m_3 \le k \le n_3 - 1 \end{cases}. \tag{A17}$$

Thus, the summation in (A14)

$$S_{\mathrm{pq}}(i,j,k) = \sum_{i'=0}^{m_1-1} \sum_{j'=0}^{m_2-1} \sum_{k'=0}^{m_3-1} g_{\mathrm{pq}}(i-i', j-j', k-k') \sum_t \varepsilon_{\mathrm{qt}}(i',j',k')E_t(i',j',k'), \tag{A18}$$

according to the discrete convolution theorem, is obtained by

$$S_{\mathrm{pq}}(i,j,k) = F^{-1}\{F[G_{\mathrm{pq}}(i',j',k')]F[P_q(i',j',k')]\}, \tag{A19}$$

where F denotes the discrete fast Fourier transform operating on i', j', and k' with three-dimensional array $n_1 \times n_2 \times n_3$, and F^{-1} is the inverse discrete fast Fourier transform.

b. Formulation of scattering parameters

As the scattering parameters are defined for the scattered field in the far field region, the following two approximations can be used:

$$e^{-jk_0R} \approx e^{-jk_0r + jk_0\hat{\mathbf{r}}\cdot\mathbf{r}'} \quad \text{and} \tag{A20}$$

$$\frac{1}{R} \approx \frac{1}{r}, \tag{A21}$$

where $\hat{\mathbf{r}}$ is the unit vector of $\mathbf{r}$. Using (A20) and (A21), the scattering field becomes

$$\mathbf{E}^s(\mathbf{r}) = \iiint_V \overline{\overline{\mathbf{H}}}\,\overline{\overline{\mathbf{X}}}(\mathbf{r}')\mathbf{E}(\mathbf{r}')\,d\mathbf{r}' \cdot \frac{1}{r}e^{-jk_0r}, \tag{A22}$$

where

$$\overline{\overline{\mathbf{H}}} = \frac{k_0^2}{4\pi}e^{jk_0r\mathbf{r}'} \cdot \begin{pmatrix} 1 - \frac{x^2}{r^2} & -\frac{xy}{r^2} & -\frac{xz}{r^2} \\ -\frac{xy}{r^2} & 1 - \frac{y^2}{r^2} & -\frac{yz}{r^2} \\ -\frac{xz}{r^2} & -\frac{yz}{r^2} & 1 - \frac{z^2}{r^2} \end{pmatrix}. \tag{A23}$$

By expressing $\overline{\overline{\mathbf{H}}}$ in spherical coordinates, where

$$x = r\sin\theta\cos\phi \quad y = r\sin\theta\sin\phi \quad z = r\cos\theta, \tag{A24}$$

(A23) becomes

$$\overline{\overline{\mathbf{H}}} = \frac{k_0^2}{4\pi} e^{jk_0(x'\sin\theta\cos\phi + y'\sin\theta\sin\phi + z'\cos\theta)} \cdot \begin{pmatrix} 1-\sin^2\theta\cos^2\phi & -\sin^2\theta\cos\phi\sin\phi & -\sin\theta\cos\phi\cos\theta \\ -\sin^2\theta\cos\phi\sin\phi & 1-\sin^2\theta\sin^2\phi & -\sin\theta\sin\phi\cos\theta \\ -\sin\theta\cos\phi\cos\theta & -\sin\theta\sin\phi\cos\theta & 1-\cos^2\theta \end{pmatrix}. \quad \text{(A25)}$$

From (A22) and (A25), the electric field of the scattered wave may be written in the far field regions as

$$\mathbf{E}^s = \mathbf{f}(\hat{\mathbf{k}}_1, \hat{\mathbf{k}}_2)\frac{1}{r}e^{-jk_0 r}, \quad \text{(A26)}$$

where $\hat{\mathbf{k}}_1$ is a unit vector directed along the propagation of the incident wave, and $\hat{\mathbf{k}}_2$ a unit vector directed from the origin to the observation point. The vector quantity $\mathbf{f}(\hat{\mathbf{k}}_1, \hat{\mathbf{k}}_2)$, called the scattering amplitude, describes the magnitude of the field and its polarization state, where

$$\mathbf{f}(\hat{\mathbf{k}}_1, \hat{\mathbf{k}}_2) = \frac{k_0^2}{4\pi} \cdot \begin{pmatrix} 1-\sin^2\theta\cos^2\phi & -\sin^2\theta\cos\phi\sin\phi & -\sin\theta\cos\phi\cos\theta \\ -\sin^2\theta\cos\phi\sin\phi & 1-\sin^2\theta\sin^2\phi & -\sin\theta\sin\phi\cos\theta \\ -\sin\theta\cos\phi\cos\theta & -\sin\theta\sin\phi\cos\theta & 1-\cos^2\theta \end{pmatrix}$$
$$\times \iiint_V \exp[jk_0(x'\sin\theta\cos\phi + y'\sin\theta\sin\phi + z'\cos\theta]\overline{\overline{\mathbf{X}}}(\mathbf{r}')\mathbf{E}(\mathbf{r}')\,d\mathbf{r}'. \quad \text{(A27)}$$

The scattering amplitude is not only a function of $\hat{\mathbf{k}}_1$ and $\hat{\mathbf{k}}_2$ but also a function of frequency, size, shape, and dielectric constant of the particle, and the polarization state of the incident wave. There is a well-known relation between extinction cross section Q_e and the scattering amplitude f in the forward direction (Saxon 1955) that is given by

$$Q_e = -\left(\frac{4\pi}{k}\right)\mathrm{Im}[\hat{\mathbf{e}} \cdot \mathbf{f}(\hat{\mathbf{k}}_1, \hat{\mathbf{k}}_2)], \quad \text{(A28)}$$

where $\hat{\mathbf{e}}$ is a unit vector of the incident wave electric field. The backscattering cross section Q_b for polarization $\hat{a}$ is defined by

$$Q_b = 4\pi|\hat{a} \cdot \mathbf{f}(\hat{\mathbf{k}}_1, -\hat{\mathbf{k}}_1)|^2. \quad \text{(A29)}$$

Other than the basic scattering parameters like Q_e and Q_b, the LDR and the differential reflectivity factor (ZDR) of the single particle are also important in radar application. These quantities can be defined in terms of the backscattering amplitudes in the main (horizontal and vertical, f_{hh} and f_{vv}) and orthogonal channels (f_{hv}) by

$$\mathrm{LDR\ (dB)} = 10\log\left[\frac{|f_{\mathrm{hv}}(\hat{\mathbf{k}}_1, -\hat{\mathbf{k}}_1)|^2}{|f_{\mathrm{hh}}(\hat{\mathbf{k}}_1, -\hat{\mathbf{k}}_1)|^2}\right] \quad \text{(A30)}$$

and

$$\mathrm{ZDR\ (dB)} = 10\log\left[\frac{|f_{\mathrm{hh}}(\hat{\mathbf{k}}_1, -\hat{\mathbf{k}}_1)|^2}{|f_{\mathrm{vv}}(\hat{\mathbf{k}}_1, -\hat{\mathbf{k}}_1)|^2}\right]. \quad \text{(A31)}$$

Significant values of LDR and ZDR can result either from the asymmetry of the particle geometry or the inhomogeneity of its dielectric properties.

REFERENCES

Bringi, V. N., R. M. Rasmussen, and J. Vivekanandan, 1986: Multiparameter radar measurements in Colorado convective storms. Part I: Graupel melting studies. *J. Atmos. Sci.,* **43,** 2545–2563.

Bruggeman, D. A. G., 1935: Berechnung verschiedener physikalischer Konstanten von heterogenen Substanzen: I. Dielectrizitatskonstanten und Leitfahigkeiten der Mischkorper aus isotropen Substanzen (Calculation of different physical constants of heterogeneous substances: I. Dielectric constants and conductances of mixtures of isotropic substances). *Ann. Phys.,* **24,** 636–679.

Catedra, M. F., R. P. Torres, J. Basterrechea, and E. Gago, 1995: *The CG–FFT Method: Application of Signal Processing Techniques to Electromagnetics.* Artech House, 361 pp.

Fabry, F., and W. Szymer, 1999: Modeling of the melting layer. Part II: Electromagnetics. *J. Atmos. Sci.,* **56,** 3596–3600.

Liao, L., and R. Meneghini, 2005: On modeling air/spaceborne radar returns in the melting layer. *IEEE Trans. Geosci. Remote Sens.,* **43,** 2799–2809.

——, ——, L. Tian, and G. M. Heymsfield, 2009: Measurements and simulations of nadir-viewing radar returns from the melting layer at X and W bands. *J. Appl. Meteor. Climatol.,* **48,** 2215–2226.

Maxwell Garnett, J. C., 1904: Colours in metal glasses and in metallic films. *Philos. Trans. Roy. Soc. London,* **A203,** 385–420.

Meneghini, R., and L. Liao, 1996: Comparisons of cross sections for melting hydrometeors as derived from dielectric mixing formulas and a numerical method. *J. Appl. Meteor.,* **35,** 1658–1670.

——, and ——, 2000: Effective dielectric constants of mixed-phase hydrometers. *J. Atmos. Oceanic Technol.,* **17,** 628–640.

Olson, W. S., P. Bauer, N. F. Viltard, D. E. Johnson, W.-K. Tao, R. Meneghini, and L. Liao, 2001a: A melting-layer model for

passive/active microwave remote sensing applications. Part I: Model formulation and comparison with observations. *J. Appl. Meteor.,* **40,** 1145–1163.

——, ——, C. D. Kummerow, Y. Hong, and W.-K. Tao, 2001b: A melting-layer model for passive/active microwave remote sensing applications. Part II: Simulations of TRMM observations. *J. Appl. Meteor.,* **40,** 1164–1179.

Ray, P. S., 1972: Broadband complex refractive indices of ice and water. *Appl. Opt.,* **11,** 1836–1844.

Sarkar, T. K., E. Arvas, and S. M. Rao, 1986: Application of FFT and the conjugate gradient method for the solution of electromagnetic radiation from electrically large and small conducting bodies. *IEEE Trans. Antennas Propag.,* **34,** 634–640.

Sassen, K., J. R. Campbell, J. Zhu, P. Kollias, M. Shupe, and C. Williams, 2005: Lidar and triple-wavelength Doppler radar measurements of the melting layer: A revised model for dark- and brightband phenomena. *J. Appl. Meteor.,* **44,** 301–312.

——, S. Matrosov, and J. Campbell, 2007: CloudSat spaceborne 94 GHz radar bright bands in the melting layer: An attenuation-driven upside-down lidar analog. *Geophys. Res. Lett.,* **34,** L16818, doi:10.1029/2007GL030291.

Saxon, D. S., 1955: Tensor scattering matrix for the electromagnetic field. *Phys. Rev.,* **100,** 1771–1775.

Stroud, D., and F. P. Pan, 1978: Self-consistent approach to electromagnetic wave propagation in composite media: Application to model granular metals. *Phys. Rev.,* **17,** 1602–1610.

Su, C. C., 1989: Electromagnetic scattering by a dielectric body with arbitrary inhomogeneity and anisotropy. *IEEE Trans. Antennas Propag.,* **37,** 384–389.